CGPG-03/3-2

CM-P00048408

Dispersion of Break Energy in the GRB Internal Shock Model

Katsuaki ASANO

Department of Earth and Space Science, Osaka University, Toyonaka, Osaka 560-0043

asano@vega.ess.sci.osaka-u.ac.jp

and

Shiho KOBAYASHI

Center for Gravitational Wave Physics, Pennsylvania State University, University Park, PA 16802

Department of Astronomy & Astrophysics, Pennsylvania State University, University Park, PA 16802

shiho@gravity.psu.edu

(Received ; accepted)

Abstract

In order to investigate the dispersion of spectral break energy in gamma-ray bursts, we simulate internal shocks including the effects of the shell splitting after shell collisions and the Thomson optical depth due to electron-positron pairs produced by synchrotron photons. We produce pseudo observational data and estimate break energy. If the distribution of initial Lorentz factors of shells has only one peak, we find that many pulses with break energy much lower than the typical observed value should be detected, while the effect of the Thomson optical depth reduces pulses with break energy > 1 MeV. If the Lorentz factor distribution has multiple peaks, the distribution of break energy can be consistent with observation.

Key words: gamma rays: bursts—radiation mechanisms: non-thermal—shock waves

1. Introduction

Gamma-ray bursts (GRBs) are short ($\lesssim 10$ sec) bursts of low energy γ-rays. One of the most important characteristics of GRB spectra is the existence of the typical break energy scale. The observed spectra of GRBs are approximated by a broken power law and the photon number spectra are approximated as $\sim \varepsilon^{-2}$ above the break energy and $\sim \varepsilon^{-1}$ below that. The standard scenario for producing GRBs is the dissipation of the kinetic energy of a relativistic flow by relativistic shocks (see, e.g., a review by Piran (1999)). The rapid temporal variability

requires that the GRB itself must arise from internal shocks within the flow. The radiation is emitted by relativistic electrons in the shocked region. The observations are well described by synchrotron emission (Cohen et al. 1997; Wijers and Galama 1999). Kobayashi et al. (1997) shows that the internal shock can reproduce the temporal structure of GRBs. A large fraction of the kinetic energy could be converted to radiation by the internal shocks (Kobayashi and Sari 2001).

The internal shock model is roughly represented by colliding shells. The collisions are considered to occur in a wide range of radius r. The energy efficiency argument requires a large dispersion of the initial Lorentz factor Γ (Kobayashi and Sari 2001; Beloborodov 2000). In spite of the large dispersions of r and Γ in the model, the apparent clustering of break energy of GRB spectra in the 50keV-1MeV range is reported in BATSE observation (Preece et al. 2000). It is strange that pulses in a burst tend to have similar break energies. The break energy distribution is in agreement with a log-normal distribution. This distribution seems to suggest small dispersions of r or Γ.

In this paper, by means of numerical simulation, we examine if the standard internal shock model can reproduce the narrow distribution of break energy. Guetta et al. (2001) showed that the internal shock model can reproduce the typical break energy. However, the dispersion of break energy has not been explained so far. In our simulation, as Guetta et al. (2001) did, we include the effects of the Thomson optical depth due to $e^{\pm}$ pairs produced by synchrotron photons. We treat the pair optical depth more precisely. In addition, our improvements in numerical simulation over those in Guetta et al. (2001) are taking into account shell splitting and the spectral energy band in observation. From our simulation we can obtain some restrictions on GRB models. In section 2 we explain the method of our simulation. In section 3 the numerical results are shown. In section 4 we summarize our results.

2. METHOD OF SIMULATION

In order to examine the distribution of break energy, we consider a spherical wind consisting of N shells. Each shell is characterized by the Lorentz factor Γ_i, mass M_i, width W_i, and radius from the center r_i. Following the evolution of the shells, there will be numerous collisions between different shells. For each collision we calculate break energy, optical depth, and flux. In order to simplify our model we idealize the situation. Some approximations are adopted in our formulation as will be seen below.

2.1. Break Energy

In this subsection we explain our method to obtain break energy. Let us consider shells with different Lorentz factors, $x \equiv \Gamma_r/\Gamma_s > 1$. The relative Lorentz factor is $\Gamma_{\rm rel} \sim (x + 1/x)/2$. The rapid and the slower shells are denoted by the subscripts r and s, respectively. We assume

that the widths of the shells are comparable in the interstellar medium (ISM) rest frame as $W_i = W$. Under these assumptions, we can obtain the ratio of the baryon number density n_r/n_s. For equal mass shells (M_i =*const.*) $n_r/n_s = 1/x$, while $n_r/n_s = 1/x^2$ for equal energy shells ($M_i\Gamma_i$ =*const.*). In this paper n and internal energy density e are measured in the fluids' rest frame.

When the rapid shell catches up with the slower one at some radius r, the forward and reverse shocks form. The shock conditions and the equality of pressures along the contact discontinuity (Sari and Piran 1995) yield

$$\frac{(\Gamma_{\rm F}-1)(4\Gamma_{\rm F}+3)}{(\Gamma_{\rm R}-1)(4\Gamma_{\rm R}+3)} = \frac{n_r}{n_s}, \tag{1}$$

where $\Gamma_{\rm F}$ and $\Gamma_{\rm R}$ are Lorentz factors of the relative motion between the regions separated by the forward shock and by the reverse shock, respectively. The equality of velocities along the contact discontinuity gives $\Gamma_{\rm R} = \Gamma_{\rm F}\Gamma_{\rm rel} - \sqrt{(\Gamma_{\rm F}^2-1)(\Gamma_{\rm rel}^2-1)}$. In the case of the equal mass shells or equal energy shells, the solution for $\Gamma_{\rm R}$ depends on only the ratio of the Lorentz factors x. The internal energy density in the shocked regions is given by

$$e = \frac{(\Gamma_{\rm R}-1)(4\Gamma_{\rm R}+3)M_r c^2}{4\pi r^2 \Gamma_r W}. \tag{2}$$

where M_r is the mass of the rapid shell.

We now consider the synchrotron emission from the shocked shells. Since the rapid shell has larger energy and lower number density in the cases of the equal mass and equal energy, the average energy per one electron in the reverse shock is larger than that in the forward shock. The reverse shock emission is more luminous and harder than the forward shock emission. Therefore, we consider only the emission from the reverse shock. The shock is assumed to accelerate electrons in the shell material into a power-law distribution: $N(\gamma_{\rm e}) \propto \gamma_{\rm e}^{-p} (\gamma_{\rm e} \geq \gamma_{\rm e,min})$. Assuming that constant fractions $\epsilon_{\rm B}$ and $\epsilon_{\rm e}$ of the internal energy go into the magnetic field and the electrons, respectively, one finds that the magnetic field and the typical random Lorentz factor of electrons are given by $B^2 \propto \epsilon_{\rm B} e$ and $\gamma_{\rm e,min} \propto \epsilon_{\rm e}(\Gamma_{\rm R}-1)$, respectively.

The synchrotron process is a very efficient radiation process. With the strong magnetic field required to produce the observed gamma-ray, the synchrotron cooling time is very short compared to the dynamical time of the shock. In this fast cooling case (Sari et al. 1998), the photon number density distribution at the fluid rest frame is given by

$$\frac{dn_\gamma(\varepsilon)}{d\varepsilon} = \frac{p-2}{2p-2}\frac{\epsilon_{\rm e} e}{\varepsilon_{\rm p}^2} \cdot \begin{cases} (\varepsilon/\varepsilon_{\rm p})^{-3/2}, & \text{for } \varepsilon < \varepsilon_{\rm p} \\ (\varepsilon/\varepsilon_{\rm p})^{-(p+2)/2}, & \text{for } \varepsilon \geq \varepsilon_{\rm p} \end{cases} \tag{3}$$

where the break energy $\varepsilon_{\rm p}$ is the typical energy of synchrotron photons emitted by electrons of $\gamma_{\rm e,min}$. Since the shocked fluid is moving with Lorentz factor $\Gamma_m \sim \Gamma_r(\Gamma_{\rm R} - \sqrt{\Gamma_{\rm R}^2-1})$, the observed break photon energy is

$$\varepsilon_{\rm p}^{\rm obs} = 610\ \epsilon_{\rm e}^2 F(x) \Gamma_{s,2} \sqrt{\Sigma/\Delta}\ \ {\rm keV}, \tag{4}$$

where $F(x)=x^{1/2}(\Gamma_{\rm R}-1)^{5/2}(4\Gamma_{\rm R}+3)^{1/2}(\Gamma_{\rm R}-\sqrt{\Gamma_{\rm R}^2-1})$. It behaves as $\sim x^2/4$ at $x\gg 1$. We have scaled the parameters as $\epsilon_{\rm B,-1}=\epsilon_{\rm B}/0.1$, $M_{48}=M_r c^2/10^{48}$ ergs, $r_{13}=r/10^{13}$ cm, $W_7=W/10^7$ cm, and $\Gamma_{s,2}=\Gamma_s/100$. We adopt $p=2.5$ here and hereafter. Since some parameters appear in the following formulae in the same combinations, we have defined two variables, a surface density $\Sigma=M_{48}/r_{13}^2$ and an effective comoving shell width $\Delta=W_7\Gamma_{s,2}/\epsilon_{\rm B,-1}$ for convenience. In our simulation we neglect the effect of the cosmological redshift on break energy.

2.2. Optical Depth due to $e^{\pm}$ Pairs

Shells are initially optically thick due to the Thomson scattering by electrons associated with baryons in the shell. For a large optical depth τ, the radiative cooling time can be estimated as $\sim \tau l/c$, where $l=W\Gamma_r/(4\Gamma_{\rm R}+3)$ is the shell width in the comoving frame. Comparing this with the cooling time due to the shell spreading $\sim l/c$, the radiated energy is negligible if $\tau \gg 1$, then, the whole internal energy is transformed back to the kinetic energy (Kobayashi and Sari 2001). Thus we could not observe the emission from it, until it comes from outside of the photosphere where the optical depth $\tau_{\rm T}=2\sigma_{\rm T}M/4\pi r^2 m_{\rm p}\sim 0.7\Sigma$ becomes unity. This is a well-know result, but the estimate may undergo a significant change in the internal shock model if we take into account $e^{\pm}$ pairs produced by the synchrotron photons (Guetta et al. 2001). In the fluid rest frame, the break photon energy $\varepsilon_{\rm p}$ is much smaller than the electron mass. However, the photon distribution extends to high energy as a power law. The pairs caused by the high energy photons may contribute significantly to the optical depth.

When a photon of energy ε interacts with a photon of ε' by a incident angle θ, the cross section of the pair creation is written by $\sigma_{\pm}=\sigma_{\rm T}f(y)$ (Berestetskii et al. 1982), where

$$f(y)=\frac{3}{16}(1-y^2)\left[(3-y^4)\ln\frac{1+y}{1-y}-2y(2-y^2)\right]. \tag{5}$$

The dimensionless value y is defined by $y^2=1-(2m_{\rm e}^2c^4)/(\varepsilon\varepsilon'(1-\cos\theta))$. The optical depth to pair-creation is given by

$$\tau_{\gamma\gamma}(\varepsilon)=\int(1-\cos\theta)d\Omega\int_{\frac{2m_{\rm e}^2c^4}{\varepsilon(1-\cos\theta)}}^{\infty}d\varepsilon'\frac{dn_\gamma(\varepsilon')}{d\varepsilon' d\Omega}\sigma_{\gamma\gamma}(\varepsilon',\varepsilon)l \tag{6}$$

$$=\sigma_{\rm T}l\frac{4(p-2)}{(p-1)(p+4)}\frac{\epsilon_{\rm e}e}{\varepsilon_{\rm p}}\left(\frac{\varepsilon\varepsilon_{\rm p}}{m_{\rm e}^2c^4}\right)^{p/2}C(p), \tag{7}$$

where

$$C(p)\equiv\int_0^1 dy(1-y^2)^{p/2-1}yf(y). \tag{8}$$

The value $C(p)$ is not sensitive to p, and $C(2.5)\sim 0.075$. Since we have used the power law distribution $dn_\gamma/d\varepsilon\propto\varepsilon^{-(p+2)/2}$ in the integration, the optical depth is overestimated for photons with high energy $\varepsilon\gtrsim 2m_{\rm e}^2c^4/\varepsilon_{\rm p}$, which interact with photons mainly in the low energy portion $dn_\gamma/d\varepsilon\propto\varepsilon^{-3/2}$. However, the exact value is not important for the high energy photons when

we estimate the number of $e^{\pm}$ pairs below, because the corrected optical depth is also large enough to annihilate all of them. For $p = 2.5$ we get

$$\tau_{\gamma\gamma}(\varepsilon) = 3.3\ \epsilon_{\rm e}^{3/2} G(x) \Sigma^{9/8} \Delta^{-1/8} \left(\varepsilon / m_{\rm e} c^2\right)^{5/4}, \tag{9}$$

where $G(x) = (\Gamma_{\rm R} - 1)^{13/8}(4\Gamma_{\rm R} + 3)^{1/8}/x^{1/8}$. Although the optical depth to pair-creation for the photons with the typical energy $\varepsilon_{\rm p} \ll m_{\rm e}c^2$ is very small, it does not necessarily imply that the number of $e^{\pm}$ pairs is negligible for the Thomson scattering. Considering that photons with energy ε interact mainly with ones with energy $\sim 2m_{\rm e}^2c^4/\varepsilon$ to produce pairs, we can estimate the optical depth due to the pairs as

$$\tau_{\pm} \sim 2\sigma_{\rm T} l \int_{\sqrt{2}m_{\rm e}c^2}^{\infty} d\varepsilon \frac{dn_{\gamma}(\varepsilon)}{d\varepsilon}(1 - e^{-\tau_{\gamma\gamma}}). \tag{10}$$

If we consider only the effect by the electrons accompanied with the baryons, the expanding ejecta becomes optically thin when the surface density $\Sigma \propto r^{-2}$ decreases down to ~ 1. However, the $e^{\pm}$ pairs produced by the synchrotron photons increase the optical depth significantly in general. Then, the ejecta is required to expand beyond $\Sigma \sim 1$ to radiate. In Figure 1 we plot the value of the surface density $\Sigma_{\rm M}$, at which the ejecta becomes optically thin, as a function of x. In order to plot Figure 1, we have numerically solved equation (1) and integrated equation (10). If we describe the system as an inelastic collisions between two masses, and a half of the internal energy is converted to pairs as Guetta et al. (2001) assumed, $\Sigma_{\rm M}$ is estimated as $\sim 0.017\epsilon_{\rm e}^{-1}\sqrt{x}/(1 + x - 2\sqrt{x})$. This approximation generally gives a smaller value.

Since the break energy $\varepsilon_{\rm p}^{\rm obs}$ is proportional to $\Sigma^{1/2}$, a collision occurring with larger Σ radiates harder photons. Then, the synchrotron photons emitted just above the radius where $\Sigma = \Sigma_{\rm M}$ are the hardest for given values of the parameters x, Δ and Γ_s. We define the maximum break energy $E_{\rm M}$ that is the break energy emitted from the radius where $\Sigma = \Sigma_{\rm M}$. The value of $E_{\rm M}$ is obtained from equation (4) with $\Sigma = \Sigma_{\rm M}$. Figure 2 depicts $E_{\rm M}$ as a function of x. We can see that the photon pair-creation effect makes $E_{\rm M}$ significantly smaller (solid lines), compared to the case without the effect (dotted lines). According to Figure 2, it is difficult to obtain a break energy more than 1 MeV for $x \leq 20$. The upper limit of break energy is determined by the Thomson optical depth due to $e^{\pm}$ pairs, and it is close to the typical observed break energy. This result agrees with Guetta et al. (2001).

In our interesting parameter region, a critical photon energy ε_{τ}, at which the optical depth $\tau_{\gamma\gamma} = 1$, is larger than $\sqrt{2}m_{\rm e}c^2$. Then, we get an approximation,

$$\tau_{\pm} \sim 300\epsilon_{\rm e}^3 G^2(x) \Sigma^{9/4} \Delta^{-1/4}, \tag{11}$$

where we neglect a logarithmic factor of ε_{τ}. We adopt this approximation in our simulation.

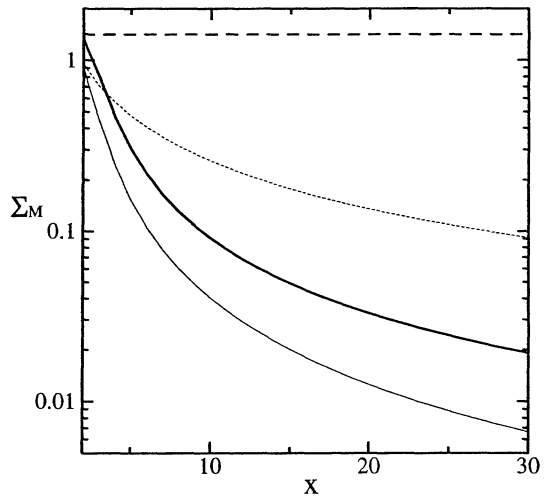

Fig. 1. Plot of Σ_M (solid line) against x. The thick and thin lines are for equal-mass and equal-energy cases, respectively. The dotted lines represent the values without pair-creation. For equal mass the value is constant as $\Sigma_M = 1.4$. Here we assume $\Delta = 1$ and $\epsilon_e = 0.5$.

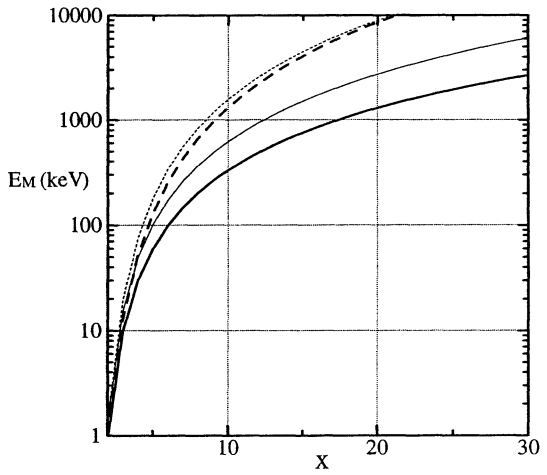

Fig. 2. Plot of E_M (solid line) against x. The dotted lines are values obtained without the process of pair-creation. The thick and thin lines are for equal-mass and equal-energy cases, respectively. Here we assume $\Delta = 1$, $\epsilon_e = 0.5$, and $\Gamma_{s,2} = 1$.

2.3. *Sampling of Break Energy*

Setting initial distributions of the Lorentz factor Γ_i and separation between shells L_i, we follow the evolution of the shells until there are no more collisions, i.e., until the shells are ordered by increasing value of the Lorentz factors. For each collision, using equations (1), (4), and (11), we estimate break energy and optical depth due to electron-positron pairs. We approximate the radiation energy as

$$E_{\rm rad} = \epsilon_{\rm e} \left(M_r(\Gamma_r - \Gamma'_m) + M_s(\Gamma_s - \Gamma'_m) \right), \tag{12}$$

where

$$\Gamma'_m = \sqrt{\frac{M_r\Gamma_r + M_s\Gamma_s}{M_r/\Gamma_r + M_s/\Gamma_s}}, \tag{13}$$

as conventionally assumed (Kobayashi and Sari 2001). After a fraction $\epsilon_{\rm e}$ of the internal energy is emitted, the shells will split, transforming the remaining internal energy back to kinetic energy. In our simulation the process of the shell splitting is basically the same in Kobayashi and Sari (2001). Introduction of the shell splitting in simulation increases the number of collisions and energy efficiency. In this paper, for simplicity, we assume that each mass and width of the shell are conserved before and after the collision. If $\tau_\pm \geq 1$, we force $\epsilon_{\rm e} = 0$. Then the collision of shells for $\tau_\pm \geq 1$ is similar to the perfectly elastic collision of pool balls.

In order to include the effect of the spectral energy band in observation, we produce pseudo observational data from our simulation. Using the spectrum of equation (3), we estimate the flux between 20 and 2000 keV from the radiation energy and break energy. We neglect the effect of the spectral sensitivity in BATSE instruments. The effective area changes only by a factor two in most part of the spectral energy band so that the effect of the sensitivity can be negligible. From the estimated flux we write light curves by the same method in Kobayashi et al. (1997). The light curves are superpositions of many pulses emitted from all collisions. The light curve peaks are identified with the peak-finding algorithm described by Li and Fenimore (1996). A peak time T_p is identified, if the peak photon flux C_p, photon fluxes C_1 ($T_1 < T_p$), and C_2 ($T_2 > T_p$) satisfy $C_p - C_{1,2} > N_{\rm var}\sqrt{C_p}$ and there are no time bins between T_1 and T_2 with photon flux higher than C_p. We adopt $N_{\rm var} = 0.3$. Results do not strongly depend on $N_{\rm var}$ (Spada et al. 2000). Each peak is identified as an "observable pulse" in our simulation. The light curve valleys are identified as the minima between two consecutive peaks. We divide the light curves in time into some regions by valleys and identify them as observed duration time of each pulse. One observable pulse may be composition of multiple pulses emitted from different collisions. For each temporal region, by attaching fluence weight, we average break energies of all pulses arrived during the period. We adopt the average break energy as "observable break energy" for each temporal region. This treatment is different from the method in actual observation. In our simulation, however, one pulse greatly overwhelms other dim pulses in most cases. Therefore, our method is harmless to determining break energy.

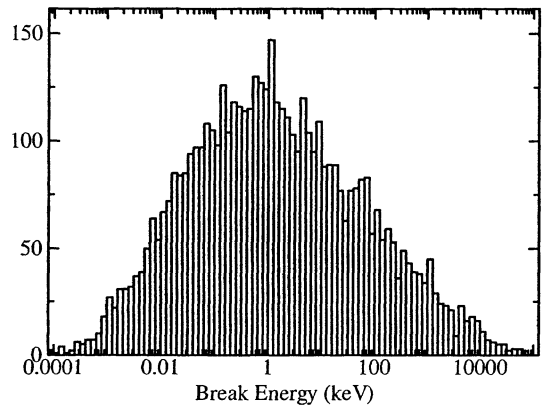

Fig. 3. Distribution of break energy for all collisions. The effect of the Thomson optical depth is neglected.

3. RESULTS OF SIMULATION

3.1. Continuous Γ-distribution

In our simulation the initial shells are assumed to have equal mass M and width W. The distributions of the initial Lorentz factor Γ_i of each shell and initial separation L_i between two consecutive shells are determined by the character of the central engine on which we have little information. In this subsection we assume that Γ_i is distributed uniformly in logarithmic space between $\log\Gamma_{\rm m}$ and $\log\Gamma_{\rm M}$ (the number distribution of shells is proportional to $1/\Gamma$). The initial separation L_i is also assumed to distribute in the same way between $\log W$ and $\log L_{\rm M}$. We perform 100 simulations with $N = 50$, $\Gamma_{\rm m} = 30$, $\Gamma_{\rm M} = 3000$, $W/c = 10^{-2}$ sec, $L_{\rm M}/c = 1$ sec, $\epsilon_{\rm e} = 0.6$, $\epsilon_{\rm B} = 0.1$, and total initial kinetic energy $E_{\rm iso} = 10^{52}$ ergs. First we neglect the effect of $\tau_{\pm}$. In Figure 3 we show a histogram of break energy for all collisions neglecting the spectral band in observation. Break energies widely distribute from optical range to 10 MeV. Apparently this result contradicts the observation. Next we take into account the Thomson optical depth. As is shown in Figure 4 the break energies above ~ 1 MeV are suppressed as we have expected in section 2.2. However, there remain many pulses with low break energy. The effect of the Thomson optical depth reduces only high-break pulses.

However, we do not observe all pulses emitted from all collisions. A dimmer pulse may be overwhelmed by other brighter pulses. Since a dimmer pulse is expected to have a lower break energy, actual observations reduces a number of pulses with low break energy. In addition a large energy fraction of emission with very low break energy may be out of the spectral energy band in observation. Therefore, we mimic BATSE observation by producing light curves from the simulations as we explained in section 2.3, and define the observable pulses and their break energies. In Figure 4, we show the result obtained from the pseudo observational data. Samples with lower break energy diminish drastically. In Figure 5 we magnify the result around BATSE band. Although the peak of the distribution is in BATSE band, the dispersion is significantly larger than observation. There are many pulses with break energy < 20 keV, which should be

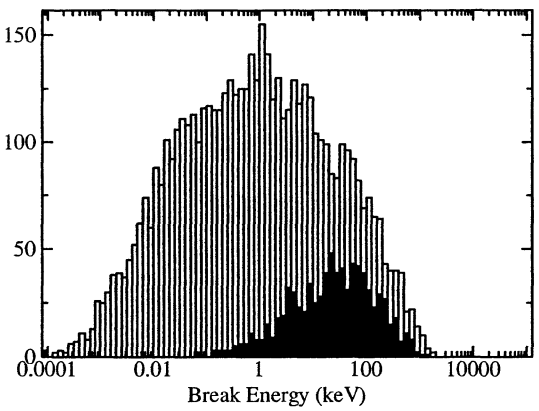

Fig. 4. Distribution of break energy for all collisions (white) and observable pulses (black). The effect of the Thomson optical depth is taken into account.

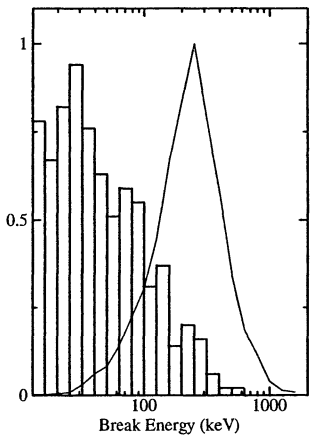

Fig. 5. Same as Fig.4 for observable pulses. Here we include the redshift effect assuming $z = 1.5$. The solid line is BATSE observation. There are many other pulses outside of this energy band. They should be counted as pulses whose spectra has no break energy.

observed as "no break" pulses. In the spectral energy band only high energy tails of bright spectra of such pulses are detected, and they make a significant peaks in the light curve.

For observable pulses in Figures 6 and 7 we show the relations between break energy and collision radius r, and between break energy and the ratio of the Lorents factors x, respectively. The collision radius and ratio x are obtained averaging in the same way as break energy. According to these figures break energy is mainly determined by the ratio x rather than r. Collisions with smaller x produce lower break energies, which causes the large dispersion of break energy. The lower limit of the collision radius in Figure 6 is determined by the Thomson optical depth.

In this model the fraction of the emission energy to the total kinetic energy is 16.9 ± 2.0 %. As Kobayashi and Sari (2001) claimed, the introduction of shell splitting increases the energy efficiency in comparison with Guetta et al. (2001) (typically a few percents). In the

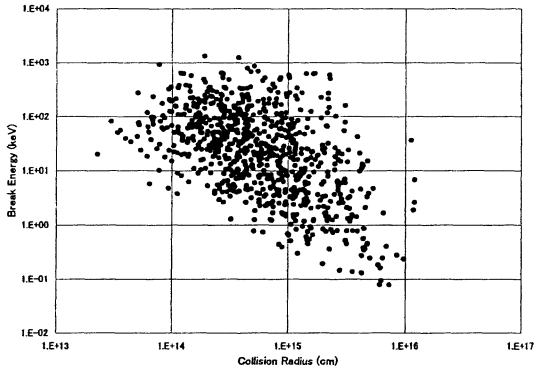

Fig. 6. Relation between break energy and collision radius.

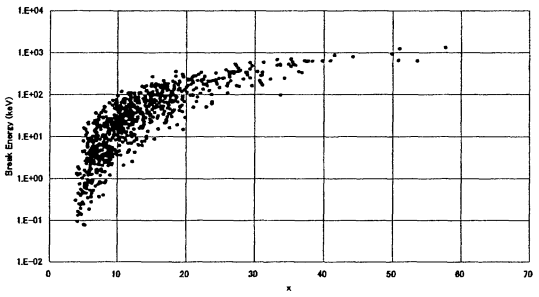

Fig. 7. Relation between break energy and the ratio x.

pseudo BATSE band the energy efficiency is 2.9 ± 0.9 %. About four times radiation energy in BATSE band are emitted outside BATSE band.

3.2. Bimodal Γ-distribution

We have attempted other types of distribution of Γ. However, as long as Γ-distribution is continuous and has only one peak, results do not change basically. The models predict many "no break" pulses. Let us consider a Γ-distribution that has a maximum at $\Gamma = \Gamma_{\rm p}$. If we randomly choose two shells in this distribution, the most probable Γs of two shells are around $\Gamma_{\rm p}$. Therefore, we cannot avoid numerous collisions with $x \sim 1$, which leads to low break energy. Of course, too small x leads to too dim emission. However, emission from a marginal value of x (~ 5) is luminous enough in spite of small break energy.

If the Γ-distribution has two peaks, the probability function of x may have a maximum at $x \gg 1$. As one example, we simulate for a bimodal Γ-distribution: one half of shells has $\Gamma = 30$ and another half has $\Gamma = 3000$ initially. The parameters are common to the former subsection. The result is shown in Figure 8. Since collisions with $\Gamma = 30$ and $\Gamma = 3000$ are dominant events in this case, break energies distribute narrowly. The result is consistent with the observation. By changing the parameters $\epsilon_{\rm e}$ etc., we can adjust the peak of the distribution to the observation more closely.

The fraction of the emission energy to the total kinetic energy is 65.1 ± 6.6 %. In

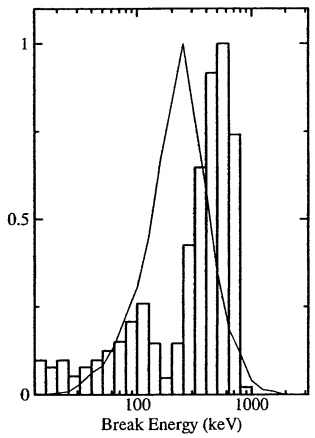

Fig. 8. Distribution of the observable break energy for the bimodal distribution. The effect of the Thomson optical depth is taken into account. Here we include the redshift effect assuming $z = 1.5$. The solid line is BATSE observation.

the pseudo BATSE band the energy efficiency is 18.7 ± 2.5 %. The bimodal distribution is advantageous to the energy efficiency also.

4. CONCLUSIONS AND DISCUSSION

Following the standard scenario of GRB, we simulate internal shocks including the effects of the shell splitting and the Thomson optical depth due to electron-positron pairs produced by synchrotron photons. We produce pseudo observational data and estimate break energy. The effect of the Thomson optical depth reduces pulses with break energy > 1 MeV, which is consistent with Guetta et al. (2001). The shell splitting effect increases the energy efficiency. However, many "no break" pulses should be observed in case of one-peak, continuous Γ-distribution. Even if we alter some assumptions (shell splitting, equal shell mass etc.) in our model, the qualitative result is basically the same. Within our simple method "no break" pulses are unavoidable, though we take into account the spectral energy band in observation. Collisions with small ratio x cause "no break" pulses. Preece et al. (2000) insists the small dispersion of break energy is not due to observational selection effects. However, we should consider the possibility of selection effects on BATSE observation henceforth.

The Γ-distribution is determined by the character of the central engine. If the initial Γ-distribution is discrete or it has multiple peaks like the bimodal distribution, the distribution of break energy can be consistent with observation. The bimodal distribution is favorable for the energy efficiency. However, we do not know if such a distribution is realistic or not.

Judging from Figure 7, if we choose pulses emitted from collisions with $x \gtrsim 10$, most of the observable break energies are in BATSE band. Therefore, if some microscopic processes prohibit collisions with $x \lesssim 10$ from emitting photons, the small dispersion of break energy can be reproduced. One of candidates for such processes is in the electron acceleration mechanism,

which is not well understood. In the standard GRB model a large fraction of the kinetic energy carried by protons is efficiently converted into that of relativistic electrons in the shocked region. However, this premise has not been theoretically proven. It is apparent that the Coulomb interaction cannot transport internal energy of heated protons into electrons to achieve energy equipartition, because the time scale of the Coulomb interaction is much longer than the dynamical time scale. In our model $x = 10$ corresponds to $\Gamma_{\rm R} = 2.57$. Therefore, the threshold $x \simeq 10$ is a border between mild-relativistic and ultra-relativistic shock. If energy of protons can be efficiently transported into electrons only for ultra-relativistic shock, the distribution of break energy can be explained. Hoshino and Shimada (2002) proposed new acceleration mechanism; shock surfing acceleration. This mechanism accelerate only electrons effectively in cases of strong shock. Such a study might explain break energy in the future.

We would like to thank T. Sakamoto for instructing information on BATSE instruments. We would also like to thank R. Preece for useful discussions, as well as providing and helping with the some of the BATSE data. K.A. was supported by the Japan Society for the Promotion of Science. S.K. thanks support through the Center for Gravitational Wave Physics, which is funded by NSF under cooperative agreement PHY 01-14375.

References

Beloborodov, A. M. 2000, ApJL, 539, L25

Berestetskii, V. B., Lifshitz, E. M., & Pitaevskii, L. P. 1982, Quantum Electrodynamics (New York: Pergamon), p. 371

Cohen, E., Katz, J. I., Piran, T., Sari, R., Preece, R. D., Band, D. L. 1997, ApJ, 488, 330

Guetta, D., Spada, M., & Waxman, E. 2001, ApJ, 557, 399

Hoshino, M., & Shimada, N. 2002, ApJ, 572, 880

Kobayashi, S., Piran, T., & Sari, R. 1997, ApJ490, 92

Kobayashi, S., & Sari, R. 2001, ApJ, 551, 934

Li, H., & Fenimore, E. E. 1996, ApJL, 469, L115

Norris, J. P. et al. 1996, ApJ, 459, 393

Piran, T. 1999, Phys. Rep., 314, 575

Preece, R. D., Briggs, M. S., Mallozzi, R. S., Pendleton, G. N., Paciesas, W. S., & Band, D. L. 2000, ApJS, 126, 1

Sari, R., & Piran, T. 1995, ApJL, 455, L143

Sari, R., Piran, T., & Narayan, R. 1998, ApJL, 497, L17

Spada, M., Panaitescu, A., & Mészáros, P. 2000, ApJ, 537, 824

Wijers, R. A. M. J., & Galama, T. J. 1999, ApJ, 523, 177